International Journal of
Molecular Sciences

MDPI

Article

RGD-Modified Kiwifruit-Derived Exosome-like Nanoparticles Loaded with si-GPAA1 Suppress the Migration and Invasion of Gastric Cancer Cells

Xiaoxin Zhang [1,2,3,*], Tiancheng Shen [2], Le Zhang [2], Yongli Huang [2], Weichen Jiang [2], Qian Hu [2], Chengdong Liang [2], Maoye Wang [2], Changlei Ning [2], Gong Guo [2], Jiahui Zhang [2], Runbi Ji [2], Min Fu [2] and Xu Zhang [1,2,*]

1 School of Basic Medical Science and Public Health, Jiangsu University, Zhenjiang 212013, China
2 Jiangsu Key Laboratory of Medical Science and Laboratory Medicine, Jiangsu University, Zhenjiang 212013, China
3 Department of Pathology, Li Ka Shing Faculty of Medicine, The University of Hong Kong, Hong Kong, China
* Correspondence: zhangxiaoxin@ujs.edu.cn (X.Z.); xuzhang@ujs.edu.cn (X.Z.)

Abstract

Gastric cancer (GC) remains a leading cause of cancer death, and metastasis is the main determinant of poor prognosis. Glycosylphosphatidylinositol (GPI) anchor attachment protein 1 (GPAA1), a subunit of the GPI transamidase complex, is overexpressed in GC and supports tumor growth and metastasis, yet no safe and efficient vehicle for delivering *GPAA1*-targeting small interfering RNA (siRNA) has been established. Here, kiwifruit-derived exosome-like nanoparticles (KDNVs) were exploited as the carrier: si-GPAA1 was loaded by electroporation and a cyclic RGD (Arg-Gly-Asp) peptide was inserted into the membrane by lipid insertion to give KDNVs-si-GPAA1-RGD. The engineered particles showed the cup-shaped morphology and colloidal properties characteristic of plant-derived vesicles and were not cytotoxic to normal gastric epithelial cells. In HGC-27 GC cells, labeled KDNVs and si-GPAA1 were internalized together and co-localized in the cytoplasm; *GPAA1* was silenced at both the mRNA and protein levels, and migration and invasion were reduced. RGD modification further improved each of these effects. RGD-modified KDNVs therefore offer a natural, food-derived platform for targeted siRNA delivery in GC.

Keywords: kiwifruit-derived exosome-like nanoparticles; RGD peptide; *GPAA1*; gastric cancer; siRNA delivery

Academic Editor: Geoffrey Brown

Received: 21 October 2026
Revised: 18 November 2026
Accepted: 23 November 2026
Published: 26 November 2026

Copyright: © 2026 by the authors. Licensee MDPI, Basel, Switzerland. This article is an open access article distributed under the terms and conditions of the Creative Commons Attribution (CC BY) license.

1. Introduction

Gastric cancer (GC) ranks among the commonest malignancies of the digestive tract and remains a leading cause of cancer death. In the most recent global estimates, it is the fifth most frequently diagnosed cancer and the fifth commonest cause of cancer mortality, with roughly 980,000 new cases and 642,000 deaths each year, and the highest rates are recorded in East Asia [1]. The burden in China is comparable: GC sits among the five leading cancers for both incidence and mortality, most patients present with advanced disease, and 5-year survival is correspondingly low [2–4]. Surgery, chemotherapy, molecularly targeted agents and immunotherapy make up the current treatment repertoire, yet outcomes remain poor. Systemic treatment is often defeated by chemoresistance and

by toxicity to normal tissue, and once the disease has metastasized, few effective options are left.

Glycosylphosphatidylinositol (GPI) anchor attachment protein 1 (GPAA1) belongs to the GPI transamidase complex, which attaches GPI anchors covalently to proteins in the endoplasmic reticulum and in doing so tethers a wide variety of proteins to the cell surface [5]. *GPAA1* is overexpressed in several human malignancies, among them breast cancer, hepatocellular carcinoma and childhood acute lymphoblastic leukemia, where it has been implicated in tumorigenesis [6–8]. In GC, Zhang et al. traced the increase to chromosomal amplification and showed that *GPAA1* promotes growth and metastasis by up-regulating metastasis-associated GPI-anchored proteins, enhancing lipid raft formation and facilitating EGFR-ERBB2 dimerization; high expression went with poor prognosis, which led the authors to propose GPAA1 as a therapeutic target. What has held the idea back is delivery: no safe and efficient vehicle for *GPAA1*-directed small interfering RNA (siRNA) has yet been established, so novel nanocarrier designs are needed.

The cytotoxic agents used in GC have three limitations that a dosage form cannot fix on its own: many are poorly water-soluble, they are cleared or degraded before reaching the tumor, and they distribute to normal tissue, so the dose that can be given is set by toxicity elsewhere rather than by what the tumor receives [9]. Nanoscale carriers address each of these at the level of formulation. Solubility is raised by encapsulation, the drug is shielded from premature degradation, and particles of this size may accumulate preferentially in tumor tissue through the enhanced permeability and retention effect [9]. The strategy is no longer only preclinical. Nanoparticle albumin-bound paclitaxel, which dispenses with the solvent responsible for hypersensitivity reactions and can therefore be given at a higher dose, was non-inferior to solvent-based paclitaxel in the phase 3 ABSOLUTE trial in GC [10,11]. What has not followed is selectivity: a 2018 survey counted fifteen passively targeted nanocarriers in clinical use and no actively targeted carrier that had completed clinical trials [12]. Closing that gap is the problem our work sets out to address.

Synthetic nanocarriers remain the default option for drug delivery in GC. Poly(lactic-co-glycolic acid) (PLGA) nanoparticles are a well-established example, and co-encapsulating docetaxel with the PI3K inhibitor LY294002 in PLGA enhanced antitumor activity against GC beyond that of the free drugs [13]. The same backbone can be extended to nucleic acid cargo: an mPEG-PLGA-b-poly(l-lysine) copolymer condensed siRNA and delivered it together with doxorubicin [14]. These systems offer defined chemistry and reproducible manufacture, yet three constraints are difficult to remove. Their preparation relies on organic solvents and repeated purification; the particles carry no recognition machinery of their own, so a targeting ligand has to be attached by chemical conjugation; and the polymer matrix provides no inherent protection against serum nucleases. Membrane-derived natural carriers address the latter two points directly, which is the reason we turned to plant-derived vesicles.

Plant-derived exosome-like nanoparticles (PELNs) have drawn steady interest as natural nanocarriers. The raw material is abundant, the vesicles are biocompatible and poorly immunogenic, and large-scale preparation is feasible [15–17]. They are also edible and biodegradable, and they arrive already carrying lipids, proteins and RNAs that may add biological activity of their own [15,18,19]. Engineering has followed two lines that complement each other. One is cargo loading, which can accommodate proteins and peptides, small interfering RNA (siRNA) or microRNA, messenger RNA and small-molecule drugs; the other is surface modification with targeting ligands such as proteins, targeting peptides or single-chain antibodies. Cargo loading decides what is delivered,

the ligand decides which cells receive it, and together they set the therapeutic window of the engineered vesicle. Several plant sources have already been tested, and a recent review catalogs their use as carriers of plant microRNAs in cancer therapy [20]. Lemon-derived nanovesicles inhibit cancer cell proliferation by activating TRAIL-mediated apoptosis and slow GC progression through reactive oxygen species (ROS) accumulation and GADD45A-mediated S-phase arrest; grape-derived exosome-like nanoparticles act on intestinal stem cells and protect against colitis; and ginger-derived nanoparticles prevent colitis-associated cancer [21–24]. Vesicles from other edible plants broaden the range: blueberry-derived exosome-like nanoparticles attenuate mitochondrial oxidative stress [25], exosome-like nanoparticles isolated from coconut water carry defined microRNA cargo [26], and grapefruit-derived nanovectors deliver both small-molecule drugs and siRNA to cells [27]. Kiwifruit has a much longer record. The pharmacopoeia Ben Cao Shi Yi lists it against joint disorders, paralysis and hemorrhoids, and the fruit and other parts of the plant are rich in triterpenoids, polyphenols, vitamin C, amino acids and minerals, a combination associated with antitumor, antioxidant and anti-inflammatory activity [28]. Kiwifruit-derived extracellular vesicles (KEVs) have proved considerably safer than conventional cationic liposomes and can carry siRNA for targeted delivery [18], and the same vesicles have been loaded with the small-molecule drug sorafenib, where their natural hepatic tropism was exploited to improve oral delivery to orthotopic liver tumors [29]. Those two studies show that kiwifruit is a workable source of nanocarriers, but the payloads tested so far have been a small molecule and a signal-transduction siRNA, and targeting has relied either on passive accumulation or on receptor-directed aptamers. Ligands aimed at the integrins that mediate tumor-cell adhesion and motility have not been tried, and PELNs in general lack active tumor-targeting capability, which limits both their specificity and their efficacy in cancer.

The cyclic RGD (Arg-Gly-Asp) peptide cRGDfK binds integrins of the αvβ3 and αvβ5 type, which tumor cells and tumor neovasculature display at high density, and this has made the motif a standard address label for tumor-targeted delivery [30]. Attaching RGD peptides to nanocarriers strengthens receptor-mediated endocytosis and raises the fraction of cargo that reaches the cytoplasm; RGD-engineered extracellular vesicles internalize more efficiently and deliver more payload in several cancer models [31,32]. The same logic underlies iRGD-modified exosomes, which have carried chemotherapeutics to integrin-positive tumors [32], and exosomes functionalized with tumor-penetrating peptides, now being explored for RNA interference (RNAi)-based cancer therapy [33,34]. For plant-derived nanovesicles, an RGD coat is therefore an obvious way to add tumor targeting that they do not naturally possess.

The work reported here proceeded in two steps. The first asked whether GPAA1 is a defensible target in human GC, using the TCGA-STAD cohort, while kiwifruit-derived exosome-like nanoparticles (KDNVs) were isolated, purified and characterized. The second loaded si-GPAA1 into KDNVs by electroporation, inserted an RGD peptide into the vesicle membrane by lipid insertion to give KDNVs-si-GPAA1-RGD, and examined the particles in the human GC line HGC-27: biocompatibility, cellular uptake, silencing of *GPAA1*, and the consequences for migration and invasion. The aim throughout was to establish experimentally whether plant-derived exosome-like nanoparticles can serve as targeted gene delivery vehicles in GC.

2. Results

2.1. Clinical and Molecular Rationale for GPAA1-Targeted Delivery in Gastric Cancer

In TCGA-STAD, *GPAA1* was expressed at a higher level in tumor tissue than in adjacent normal mucosa. (Figure 1A), so the protein is both readily detectable and upregulated in gastric cancer (GC). Since the delivery platform depends on an RGD motif, the corresponding integrin subunits also had to be present. ITGB1, ITGAV and ITGB5 were each significantly upregulated in tumor tissue (Figure 1B), consistent with the presence of RGD-binding integrin complexes in GC and supporting the rationale for integrin-targeted delivery, although transcript-level data do not resolve the abundance of individual αvβ3 or αvβ5 heterodimers.

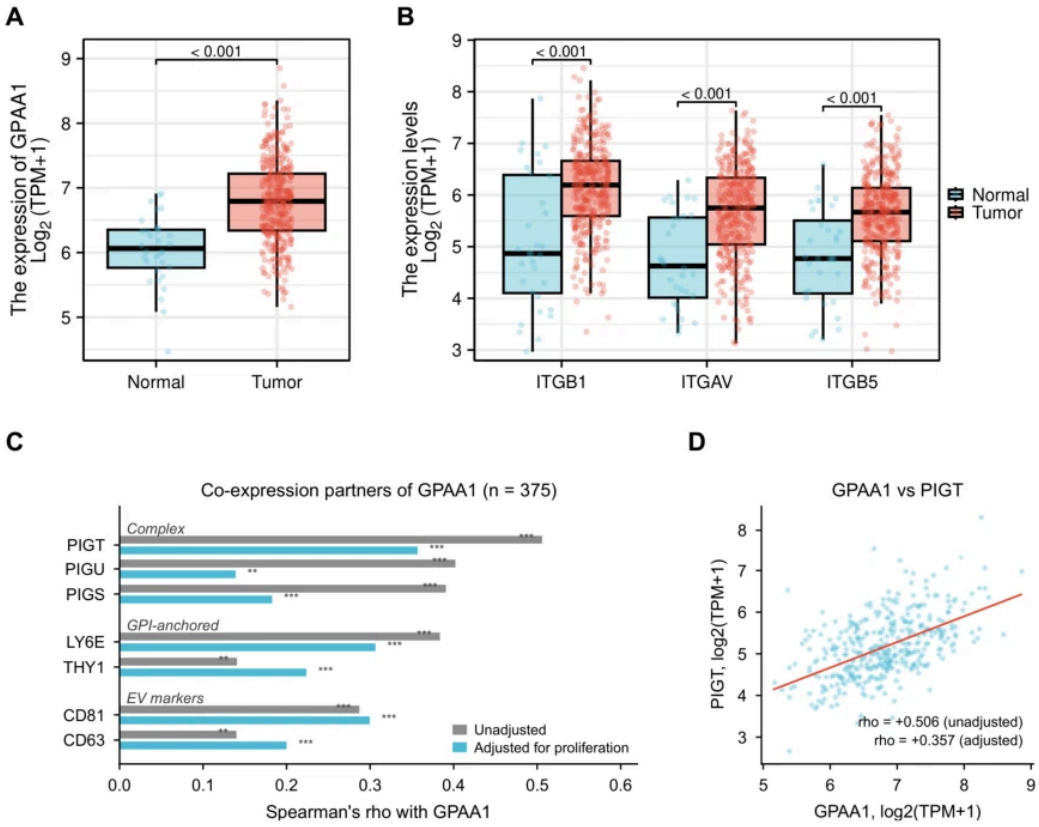

Figure 1. *GPAA1* expression, RGD-binding integrins and co-expression partners in gastric cancer. (**A**) *GPAA1* expression in tumor tissue (n = 375) versus adjacent normal mucosa (n = 32) in the TCGA-STAD cohort (unpaired Student's *t*-test). (**B**) Expression of the RGD-binding integrin subunits ITGB1, ITGAV and ITGB5 in the same cohort (Mann–Whitney U test). (**C**) Spearman's rank correlation between *GPAA1* and its co-expression partners within tumors (n = 375): the remaining members of the GPI transamidase complex (PIGT, PIGU, PIGS), the GPI-anchored proteins LY6E and THY1, and the extracellular vesicle markers CD81 and CD63. Asterisks denote the significance of each coefficient (*** $p < 0.001$, ** $p < 0.01$); all coefficients shown reached $p < 0.01$ both before and after adjustment. (**D**) Representative scatter plot of *GPAA1* versus PIGT, with the least-squares fit in red. Boxes in (**A**,**B**) show the median and interquartile range, whiskers the 1.5 × IQR range, and dots individual samples. Expression values are $\log_2(\text{TPM} + 1)$. Correlations are reported as measures of association only and do not imply regulation.

How *GPAA1* expression relates to that of its functional partners was examined next. Within the GPI transamidase complex, *GPAA1* correlated positively with PIGT, PIGU and PIGS (Figure 1C). *GPAA1* also tracked the proliferation/chromosomal instability

(CIN) index, so partial correlation was used to remove that contribution. After adjustment, the PIGT association remained robust (partial ρ = 0.357, $p = 1.0 \times 10^{-12}$), while those with PIGU and PIGS weakened.

Among GPI-anchored surface proteins, LY6E and THY1 stayed positively associated with *GPAA1* after adjustment for the proliferation/CIN index (adjusted ρ = 0.306 and 0.224, respectively). In both cases, the coefficient grew rather than shrank, most obviously for THY1, whose expression was itself weakly and inversely related to the proliferation/CIN index. The extracellular vesicle (EV)-associated markers CD81 and CD63 behaved in the same way (adjusted ρ = 0.300 and 0.200), although their ties to the proliferation/CIN index were weak (Figure 1C,D).

Such co-expression patterns are descriptive only. GPI anchoring and EV cargo sorting are post-translational events, and transcript-level correlations cannot resolve them, so no direct regulatory relationship should be read into these numbers. What the analysis does support is that *GPAA1* is overexpressed in GC and that an RGD-mediated delivery strategy is biologically reasonable in this disease. The associations with the GPI transamidase subunits, with GPI-anchored surface proteins and with EV markers supply additional molecular context for the delivery experiments that follow.

2.2. Isolation and Characterization of KDNVs

Electron microscopy showed the isolated KDNVs as cup-shaped or vesicular membrane-bound structures with clear outlines and a bilayer-like appearance (Figure 2A), the morphology expected of exosome-like nanoparticles. The BCA assay put the protein concentration of the suspension at approximately 1.0 μg/μL, so a considerable amount of vesicle-associated protein can be recovered from kiwifruit juice by this isolation procedure. Nanoparticle tracking analysis gave a mean peak diameter of 175.3 nm and a particle concentration of 4.9×10^{11} particles/mL (Figure 2B), and the Zeta potential, measured by electrophoretic light scattering, was −31.94 ± 0.49 mV (Figure 2C). Vesicles of this size are within the range that permits efficient cellular internalization, and the negative surface charge, typical of plant-derived nanovesicles, contributes to colloidal stability and dispersion. Morphology and physicochemical data together indicate that kiwifruit-derived exosome-like nanoparticles were isolated successfully and provide the basis for their subsequent engineering.

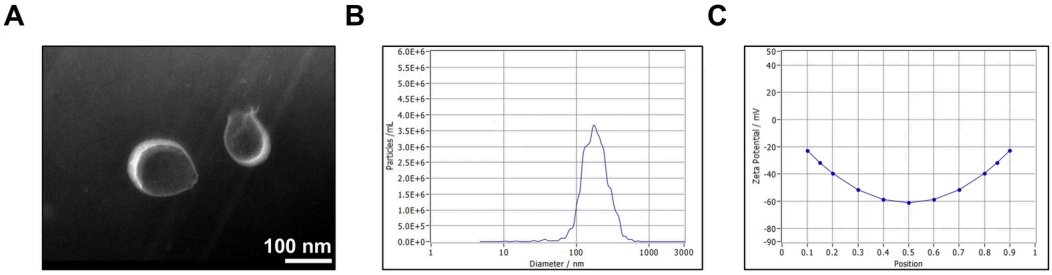

Figure 2. Isolation and characterization of KDNVs. (**A**) Transmission electron microscopy image of KDNVs showing typical cup-shaped morphology (scale bar, 100 nm); (**B**) particle size distribution of KDNVs determined by NTA; (**C**) Zeta potential of KDNVs determined by electrophoretic light scattering.

2.3. Engineered KDNVs Exhibit No Obvious Cytotoxicity in Normal Gastric Epithelial Cells

A gene delivery vehicle has to be tolerated before it can be useful, so the toxicity of KDNVs and of the RGD-modified formulation toward non-malignant gastric epithelium was assessed in the normal gastric epithelial cell line GES-1 before the delivery experiments. Annexin V-FITC/PI double-staining flow cytometry showed no significant differ-

ence in the apoptosis rate of the normal human gastric epithelial cell line GES-1 among the PBS, DMSO, KDNVs, KDNVs+RGD and free cRGDfK groups after 24 h (Figure 3A). Metabolic activity was assessed independently by CCK-8 over five days in the same groups and under the same conditions, and relative cell viability did not differ significantly between any treatment group and the PBS control at any time point (Figure 3B). Neither the vesicles nor the RGD modification therefore produced an obvious cytotoxic effect in GES-1 cells, indicating that the engineered nanoparticles are well tolerated by non-malignant gastric epithelium.

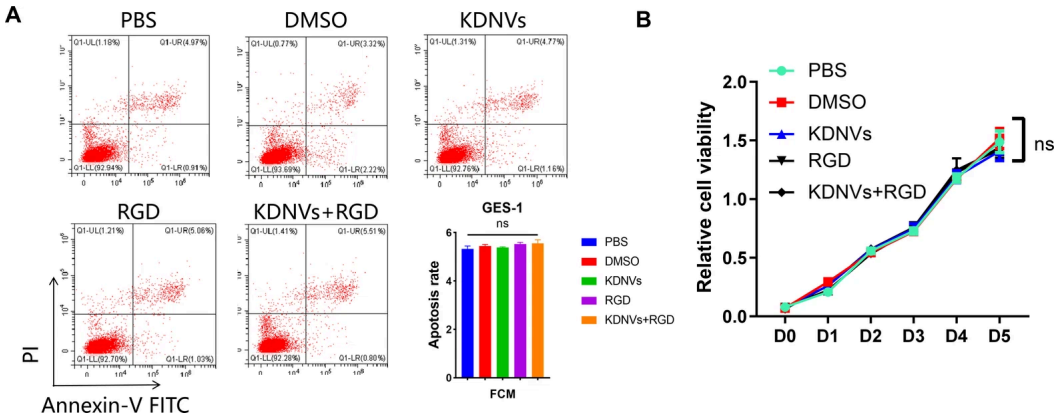

Figure 3. Cytotoxicity of KDNVs and the RGD-modified formulation in GES-1 cells (normal human gastric epithelial cells). (**A**) Annexin V-FITC/PI flow cytometry of cells treated with PBS, DMSO, KDNVs, KDNVs+RGD or free cRGDfK for 24 h, with the corresponding apoptosis rates shown as a bar graph. (**B**) Relative cell viability measured by CCK-8 from day 0 to day 5 in the same groups (n = 5 per time point; ns, not significant).

2.4. Cellular Uptake and Co-Localization of Engineered KDNVs

Silencing depends on how much cargo reaches the cytoplasm, so intracellular delivery was examined directly. After incubation, HGC-27 cells contained both DiI-labeled KDNVs and FAM-labeled si-GPAA1 , and the two signals largely overlapped in the cytoplasm; against the DAPI-stained nuclei , the merged images showed a clear spatial distribution (Figure 4). si-GPAA1 thus entered GC cells together with KDNVs and co-localized with them, which is the behavior required of an efficient gene carrier.

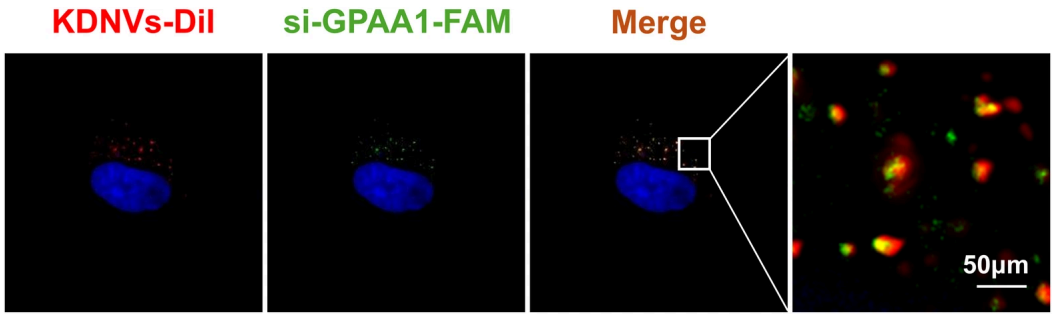

Figure 4. Fluorescence microscopy images showing the cellular uptake and co-localization (yellow) of DiI-labeled KDNVs (red) and FAM-labeled si-GPAA1 (green) in HGC-27 cells. Nuclei were stained with DAPI (blue).

2.5. Knockdown Efficiency of GPAA1 Mediated by Engineered KDNVs

To determine whether the delivered siRNA remains active after intracellular trafficking, *GPAA1* mRNA was measured by RT-qPCR. Relative to KDNVs-si-NC, *GPAA1* mRNA was significantly lower after KDNVs-si-GPAA1 and lower again after KDNVs-si-

GPAA1-RGD (Figure 5A). Western blotting of the 68 kDa GPAA1 band agreed with the transcript data: protein was markedly reduced by KDNVs-si-GPAA1 and reduced further by KDNVs-si-GPAA1-RGD, with GAPDH (36 kDa) as the loading control (Figure 5 B). Silencing was therefore achieved at both the mRNA and protein levels, and the RGD coat improved it, as would be expected if integrin binding increases cellular uptake.

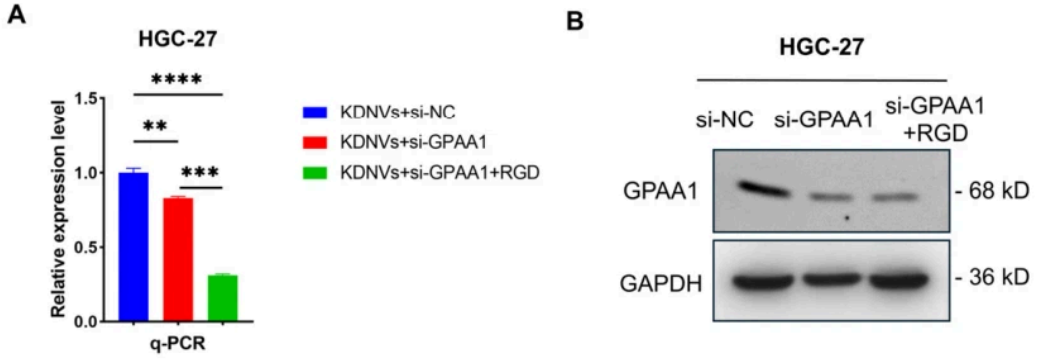

Figure 5. Knockdown efficiency of *GPAA1* in HGC-27 cells treated with KDNVs-si-NC, KDNVs-si-GPAA1, or KDNVs-si-GPAA1-RGD for 48 h. (**A**) RT-qPCR analysis of *GPAA1* mRNA expression (n = 3; each siRNA group vs. si-NC, two-tailed unpaired *t*-test; ** $p < 0.01$, *** $p < 0.001$, **** $p < 0.0001$); (**B**) Western blotting analysis of GPAA1 (68 kDa) protein expression, with GAPDH (36 kDa) as the loading control.

2.6. Engineered KDNVs Inhibit the Migration and Invasion of HGC-27 Cells

The consequence of *GPAA1* silencing for the malignant phenotype was then assessed in Transwell assays. Significantly fewer KDNVs-si-GPAA1-treated cells crossed the membrane than KDNVs-si-NC-treated cells, and fewer still crossed after KDNVs-si-GPAA1-RGD ($p < 0.05$) (Figure 6). Invasion through Matrigel fell in the same order (Figure 6). Knocking down *GPAA1* therefore restricted the migration and invasion of GC cells, and RGD modification strengthened the effect, most likely by improving delivery.The construction of the two formulations and the route by which the RGD ligand directs them to GC cells are summarized (Figure 7).

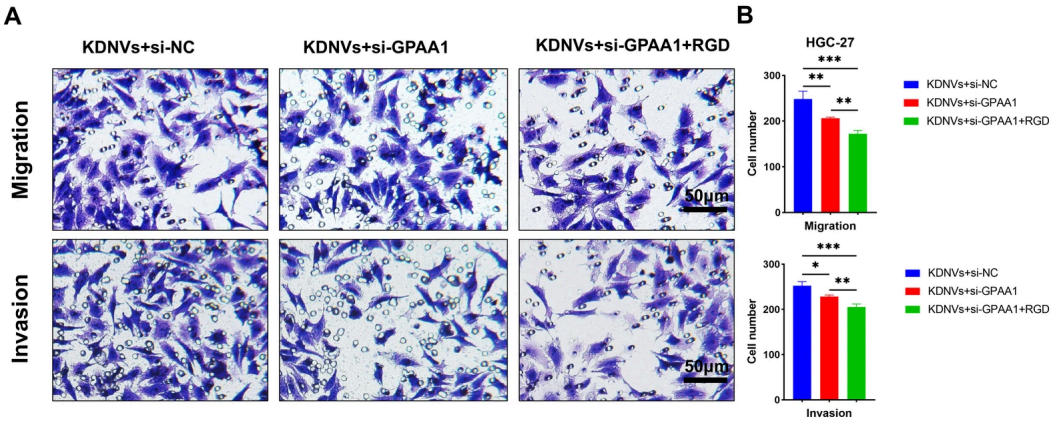

Figure 6. Effects of engineered KDNVs on the migration and invasion of HGC-27 cells. (**A**) Representative imagesof migratedand invadedcells after treatment with KDNVs-si-NC, KDNVs-si-GPAA1, or KDNVs-si-GPAA1-RGD; scale bar:50μm (**B**) numbers of migrated and invaded cells, counted in five randomly selected fields per membrane (one-way ANOVA with SNK post hoc test; n = 3; * $p < 0.05$, ** $p < 0.01$, *** $p < 0.001$).

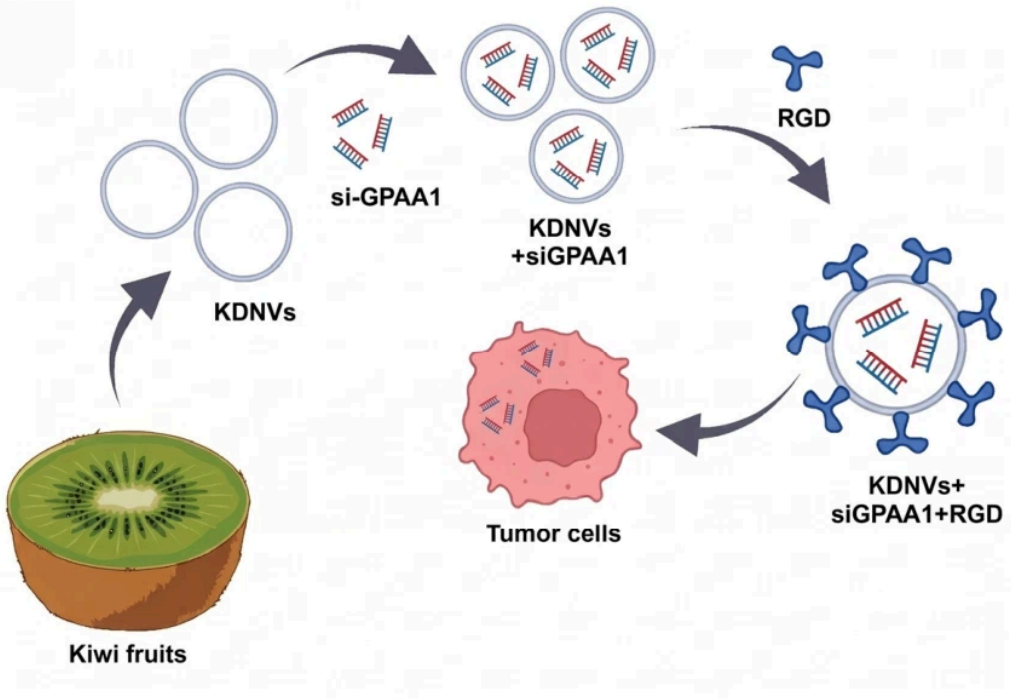

Figure 7. Schematic illustration of the construction and targeted delivery of engineered kiwifruit-derived nanovesicles. KDNVs are isolated from kiwifruit and loaded with si-GPAA1 by electroporation to give KDNVs-si-GPAA1, which are then surface-decorated with an RGD peptide by lipid insertion to generate KDNVs-si-GPAA1-RGD. The RGD ligand is designed to recognize integrins that are overexpressed on the surface of gastric cancer cells, thereby promoting the uptake of the engineered nanovesicles by tumor cells and the intracellular delivery of si-GPAA1.

3. Discussion

Advanced GC responds poorly to systemic therapy, partly because few agents act on the molecular events that drive progression and partly because of delivery. GPAA1, an enzymatic subunit of the GPI transamidase complex, behaves as an oncogene in several tumor types [5–8], and our TCGA-STAD analysis places it in the same category in GC: expression was elevated and tracked that of the other transamidase subunits and of the extracellular vesicle markers. We therefore built an RGD-modified delivery system on kiwifruit-derived exosome-like nanoparticles (KDNVs) and showed that it silences *GPAA1* and reduces the migration and invasion of HGC-27 cells.

Plant-derived exosome-like nanoparticles have practical advantages that are hard to reproduce synthetically. Vesicles from lemon [21,22], ginger [24] and *Dipsacus asperoides* [35] are well tolerated and show antitumor activity, grape-derived vesicles act on intestinal stem cells and protect against colitis [23], and KEVs tolerate a sevenfold higher dose than cationic liposomes and can carry siRNA [18]. The particles isolated here fit this picture: cup-shaped morphology, a diameter in the small-vesicle range and a negative surface charge, with no cytotoxicity toward normal gastric epithelial cells. The isolation procedure is also workable, recovering approximately 1 μg/μL of vesicle protein from kiwifruit juice.

Two earlier studies of kiwifruit-derived nanocarriers provide the closest comparison. Huang et al. loaded siSTAT3 into cation-free KEVs and added EGFR targeting by hydrophobic aptamer anchoring, reversing chemoresistance in EGFR-mutant non-small cell lung cancer [18]; Fang et al. encapsulated sorafenib in KEVs and exploited their hepatic tropism to improve oral delivery in hepatocellular carcinoma [29]. Our design differs in three respects. The targeting motif is the cyclic RGD peptide cRGDfK rather than

an aptamer or passive accumulation, and it is installed by lipid insertion, which avoids the covalent coupling and purification that aptamer conjugation requires. The cargo silences *GPAA1*, an enzymatic subunit of the GPI transamidase complex, rather than a downstream signaling effector, so it acts on the assembly of the whole repertoire of GPI-anchored surface proteins. And the phenotype interrogated is migration and invasion rather than proliferation or drug sensitivity, which matches the metastatic step that determines GC mortality. To our knowledge, no kiwifruit-derived nanocarrier has previously been directed by an RGD peptide, and none has used the GPI transamidase complex as the silencing target of a plant-derived delivery system.

Beyond vesicle-based platforms, edible plant materials have been used more generally to improve the stability and oral availability of poorly soluble bioactives. Nanotechnology-based formulation has improved the bioavailability of diet-derived flavonoids [36], garlic organosulfur compounds [37] and citrus flavonoids [38], and self-assembled prodrug nanoparticles have done the same for capsaicin while reducing its gastrointestinal irritation [39]; nonionic surfactant vesicles raised the oral bioavailability of ginsenoside Rb1 [40], and bacterial extracellular vesicles are being explored for intestinal delivery [41]. These approaches share a constraint that applies here as well: the carrier must be matched both to the properties of the cargo and to the barrier it has to cross.

Untargeted plant-derived vesicles have limited tumor selectivity. Integrins such as αvβ3 and αvβ5 are highly expressed on tumor cells and tumor neovasculature, which makes them attractive addresses for targeted delivery [30], and RGD peptides have long been used to functionalize nanocarriers, exosomes included [30–32]. Gečys et al. showed that RGD modification increases the internalization of extracellular vesicles by glioblastoma cells [31], and Tian et al. delivered doxorubicin to integrin-positive tumors with iRGD-functionalized exosomes [32]. Chemical conjugation of such ligands usually requires covalent cross-linking and purification, both of which can compromise membrane integrity and the activity of the cargo; lipid insertion instead exploits the hydrophobic interaction between the lipid moiety of the conjugate and the bilayer and proceeds under mild conditions. Co-incubating DSPE-PEG2000-cRGDfK with siRNA-loaded KDNVs was sufficient to confer integrin targeting, and the procedure requires no covalent coupling and only ultrafiltration to remove unbound ligand, which should favor scale-up. How stable the inserted peptide remains on the vesicle surface, and how decoration density relates to delivery efficiency, still require systematic optimization.

si-GPAA1 was loaded by electroporation, the usual method for introducing siRNA into exosomes and other nanovesicles [33,34]. Co-localization confirmed that KDNVs delivered si-GPAA1 into the cytoplasm, and knockdown experiments showed that the RGD-modified form silenced *GPAA1* more effectively. Physical loading methods give variable encapsulation efficiency and can leave cargo aggregated outside the vesicle, and both parameters are considered further in the Limitations. Downstream of silencing, regulation of GPI-anchored protein expression and of downstream signaling is the likely route. Zhang et al. showed that GPAA1 up-regulates metastasis-associated GPI-anchored proteins, enhances lipid raft formation and promotes EGFR-ERBB2 dimerization [5], and GPAA1 has also been reported to act through c-myc in acute lymphoblastic leukemia [8]. Reduced GPI anchor biosynthesis would be expected to destabilize adhesion and receptor platforms at the membrane and to attenuate migratory and invasive capacity, which is what HGC-27 cells displayed.

These results extend the use of plant-derived exosome-like nanoparticles as nucleic acid carriers. PELNs can be engineered with targeting ligands and loaded with siRNAs, miRNAs or chemotherapeutic agents [34,42,43]; grapefruit-derived nanovectors delivered miR-17 intranasally and inhibited brain tumor progression [42], and ginger-derived

nanovectors loaded with siRNA were effective in colitis models [43]. Against synthetic lipid nanoparticles, plant vesicles offer natural origin, low immunogenicity and scalable production [15,18]. Translation nevertheless faces obstacles common to the field: heterogeneity between batches and between plant sources, limited standardization of isolation and characterization protocols, and no reproducible framework for evaluating batch-to-batch consistency.

Size deserves to be stated explicitly, because a mean diameter of 175 nm can be read as too large for a systemically administered carrier to survive. The thresholds point the other way. Renal filtration is restricted to particles with a hydrodynamic diameter below about 5.5 nm, a threshold established in a quantum-dot model [44], so a vesicle of this size is not removed by the kidney, and particles in the 100–200 nm range are at the same time large enough to extravasate through the leaky vasculature of permissive tumors and to be internalized efficiently by cells [45]. The constraint that does apply is phagocytic: hepatic and splenic macrophages take up particles of this size more readily than small ones, and above roughly 100 nm, the mononuclear phagocyte system, rather than filtration, is the dominant route of clearance [45]. Size alone therefore does not decide whether these vesicles reach a tumor; what decides it is how readily macrophages recognize them, which is why the surface was kept negatively charged and hydrophilic, and why the targeted form presents its ligand on a PEG2000 spacer.

Two routes exist for loading a vesicle, and the choice between them is set by the source of the vesicle rather than by preference. In exogenous loading, the cargo is introduced after isolation; in endogenous loading, the producer cell is engineered so that the cargo is packaged during vesicle biogenesis [46,47]. The exogenous repertoire is broad—passive incubation for hydrophobic molecules, electroporation, sonication, extrusion, freeze–thaw cycling and saponin permeabilisation—and each method trades loading yield against membrane integrity [46]. Endogenous loading can avoid that trade-off, because the cargo enters the lumen through the same sorting pathway that normally populates the vesicle, and exosomes naturally carry mRNA and microRNA, which is the basis of the approach [48]. For kiwifruit-derived vesicles, this route is not available. The starting material is fruit juice rather than a cultured producer cell, so there is no cell to engineer and loading has to be performed on the isolated particle. Within that constraint, electroporation was selected, because it suits siRNA, requires no hydrophobic modification of the cargo and is the method most widely applied to vesicles of this kind [33,34]. Its weaknesses—variable efficiency, aggregation of cargo outside the vesicle and transient membrane disruption—are documented for electroporation [49] and are considered further in the Limitations.

Several points mark out the next stage of this work. All experiments were performed in vitro, so the biodistribution, tumor-targeting efficiency and antitumor efficacy of the engineered KDNVs await evaluation in GC-bearing mice. The route through which GPAA1 restrains migration and invasion is most likely to run through the GPI-anchored surface proteins whose display it governs, and dissecting that route is the direct continuation of the silencing data reported here. Two features of the loading step remain open to closer analysis: the proportion of si-GPAA1 that resides within the vesicle lumen rather than at its surface, and the effect of electroporation on membrane integrity, both of which call for fractionation or single-particle methods. Uptake was followed by co-localization imaging and by its functional consequence, the extent of *GPAA1* silencing, and flow-cytometric quantification will express the RGD contribution as a fold change. The transcriptomic analyses rest on a single public cohort and describe associations, so independent cohorts and functional perturbation will be needed to test causality. Working through these questions in GC-bearing mouse models is the next stage of this work.

4. Materials and Methods

4.1. Reagents and Instruments

DMEM medium, fetal bovine serum (FBS) and trypsin were purchased from Gibco (Waltham, MA, USA); penicillin–streptomycin, DSPE-PEG2000-cRGDfK and the Annexin V-FITC/PI apoptosis detection kit from Beyotime Biotechnology (Shanghai, China). si-GPAA1, si-NC and FAM-labeled si-GPAA1 (si-GPAA1-FAM) were synthesized by GenePharma (Shanghai, China). DiI fluorescent dye was from Invitrogen (Carlsbad, CA, USA) and DAPI staining solution from Solarbio (Beijing, China). Antibodies against GPAA1 (10104-1-AP, 1:1000) and GAPDH (60004-1-Ig, 1:2000) were from Proteintech (Wuhan, China), and the corresponding horseradish peroxidase-conjugated secondary antibodies were from Cell Signaling Technology (Danvers, MA, USA). PVDF membranes were from Millipore (Burlington, MA, USA) and Matrigel from Corning (Corning, NY, USA). The si-GPAA1 duplexes are listed in Table 1; si-GPAA1 #1 gave the highest knockdown efficiency and was used in all subsequent experiments. Instruments were a transmission electron microscope (Philips, Eindhoven, The Netherlands), a NanoSight NS300 nanoparticle tracking analyzer (Malvern Panalytical, Malvern, UK), a Zetasizer (Malvern Panalytical, Malvern, UK), a flow cytometer (BD Biosciences, San Jose, CA, USA), a fluorescence microscope (Nikon, Tokyo, Japan), an electroporator (Bio-Rad, Hercules, CA, USA) and a chemiluminescence imaging system (GE Healthcare, Chicago, IL, USA).

Table 1. Sequences of the si-GPAA1 duplexes used in this study.

Name	Sense (5′→3′)	Antisense (5′→3′)
si-GPAA1 #1	CCTTGACCTGCTCAATCTC	GAGATTGAGCAGGTCAAGG
si-GPAA1 #2	TAGCTTCCGCCAGTACAAG	CTTGTACTGGCGGAAGCTA
si-GPAA1 #3	TGAGACCCACGAGCGCTATAT	ATATAGCGCTCGTGGGTCTCA

4.2. Cell Line and Culture

The human GC cell line HGC-27 was obtained from the Cell Bank of the Chinese Academy of Sciences (Shanghai, China) and maintained in DMEM supplemented with 10% FBS, 100 U/mL penicillin and 100 μg/mL streptomycin at 37 °C in a humidified atmosphere containing 5% CO_2. The normal human gastric epithelial cell line GES-1 was obtained from the Cell Bank of the Chinese Academy of Sciences (Shanghai, China) and cultured under the same conditions. Cells in logarithmic growth were used for all experiments.

4.3. Isolation and Purification of KDNVs

Fresh kiwifruits were bought at a local market in Zhenjiang, China, in March 2025, then peeled, washed and juiced. The juice was cleared by sequential centrifugation at 200× *g* for 10 min, 2000× *g* for 20 min and 10,000× *g* for 30 min at 4 °C, and the supernatant was retained. It was ultracentrifuged at 100,000× *g* for 60 min at 4 °C and the pellet resuspended in PBS. This suspension was layered onto a sucrose density gradient (8%, 15%, 30%, 45% and 60%) and centrifuged at 100,000× *g* for 60 min at 4 °C. The fraction between the 30% and 45% sucrose layers was collected, resuspended in a large volume of PBS and washed by a second ultracentrifugation. The resulting KDNVs were sterilized by filtration through a 0.22 μm filter and stored at −80 °C until use.

4.4. Characterization of KDNVs

For transmission electron microscopy (TEM), an appropriate volume of the KDNV

suspension was dropped onto a carbon-coated copper grid, adsorbed for 3 min, negatively stained with phosphotungstic acid (pH 6.8) at room temperature and dried under an incandescent lamp before observation. Particle size distribution and particle concentration were determined by nanoparticle tracking analysis (NTA) on a NanoSight NS300 system, and Zeta potential was measured by electrophoretic light scattering on a Zetasizer (Malvern Panalytical, Malvern, UK). Samples were diluted 1:1,000 in 0.22 μm-filtered PBS to reach the optimal operating concentration of 10^8–10^9 particles/mL, and measurements were recorded at 25.0 °C from three independent 60-s video captures at 30 frames per second, with optimized camera level and detection threshold settings. Plant-derived vesicles lack the canonical tetraspanin markers used to characterize mammalian EVs, so KDNV identity was established by morphology, size distribution, surface charge and protein content, in line with MISEV guidance for plant-derived vesicles. The protein concentration of the KDNV suspension was determined with the BCA assay (Pierce™ BCA Protein Assay Kit, Cat# 23225, Thermo Fisher Scientific, Waltham, MA, USA).

4.5. Bioinformatic Analysis of GPAA1 Expression, Integrins and Co-Expression Partners

Expression and clinical data for the stomach adenocarcinoma cohort (TCGA-STAD; 375 tumor and 32 adjacent normal samples) were obtained from the NCI Genomic Data Commons (https://portal.gdc.cancer.gov (accessed on16 September 2026)). STAR-derived TPM values were $\log_2$(TPM + 1)-transformed without additional filtering. Normality (Shapiro–Wilk test) and homogeneity of variance (Levene's test) were evaluated; *GPAA1* met both assumptions and was compared by an unpaired Student's *t*-test, whereas ITGB1, ITGAV and ITGB5 were compared by the Mann–Whitney U test. ITGB3 was excluded because of low expression (median $\log_2$(TPM + 1) = 1.98 in tumors). Tumor co-expression was assessed by Spearman's rank correlation. *GPAA1* expression correlated with cell-cycle activity (Spearman rho = +0.473 with the proliferation/CIN index, $p = 2.4 \times 10^{-22}$; the index being defined as the mean z-score of MKI67, CCNE1, AURKA, FOXM1, TOP2A and E2F1), so rank-based partial correlations were calculated from ordinary-least-squares residuals. No covariate adjustment was applied in panels A and B. Statistical significance was set at $p < 0.05$. Analyses and plots were produced in R (v4.2.1, ggplot2 v3.4.4) and Python (v3.13, SciPy v1.18).

4.6. Construction of Engineered KDNVs

si-GPAA1 was loaded by electroporation. KDNVs were mixed with si-GPAA1 (or si-NC) at a protein-to-RNA weight ratio of 10:1 (*w*/*w*) in pre-chilled electroporation buffer (1.15% glucose in sterile PBS, pH 7.4), transferred to a 0.2 cm electroporation cuvette and pulsed once at 400 V and 125 μF (Gene Pulser Xcell; Bio-Rad Laboratories, Hercules, CA, USA). After the pulse the samples were held at 37 °C for 30 min to allow membrane recovery, and free siRNA was removed by ultrafiltration (100 kDa molecular weight cutoff, MWCO; Amicon Ultra, Millipore, Burlington, MA, USA) to give KDNVs-si-GPAA1 and KDNVs-si-NC.

For RGD surface modification, DSPE-PEG2000-cRGDfK was co-incubated with KDNVs-si-GPAA1 at a final concentration of 10 μM for 45 min at 37 °C under gentle agitation, which allowed the hydrophobic moiety of the conjugate to insert into the lipid bilayer; free peptide was removed by ultrafiltration (100 kDa MWCO) to give KDNVs-si-GPAA1-RGD. For uptake experiments, KDNVs were labeled with the lipophilic dye DiI before engineering (final concentration 2 μM, 37 °C, 20 min, in the dark), followed by ultrafiltration to remove unconjugated dye.

4.7. Cytotoxicity Assays

Logarithmically growing GES-1 cells were seeded in 6-well plates at 2.5 × 10^5 cells/well in 2 mL of complete medium and allowed to adhere overnight. They were then treated with PBS (vehicle control), 0.1% (*v*/*v*) DMSO, KDNVs (30 μg/mL protein equivalent), KDNVs+RGD (RGD-modified KDNVs, 30 μg/mL protein equivalent) or free cRGDfK (10 μM) for 24 h. Adherent and detached floating cells were then harvested together, washed twice with cold PBS and stained with Annexin V-FITC and propidium iodide (PI) according to the manufacturer's instructions. The apoptosis rate of each group was analyzed immediately by flow cytometry (BD FACSCanto II), and the percentage of apoptotic cells (Annexin V+/PI- and Annexin V+/PI+) was quantified in FlowJo software (v10.8.1).

Cell viability was measured separately with a CCK-8 assay (Beyotime Biotechnology, Shanghai, China). GES-1 cells were seeded in 96-well plates at 3 × 10^3 cells per well; allowed to adhere overnight; and then treated with PBS, 0.1% (*v*/*v*) DMSO, KDNVs, KDNVs+RGD or free cRGDfK at the concentrations given above. At each time point from day 0 to day 5, CCK-8 reagent was added to the wells and the plates were incubated for 1 h at 37 °C, after which the absorbance was read at 450 nm on a microplate reader. Five replicate wells were used for each group at each time point, and relative cell viability was calculated as the ratio of the absorbance of each treatment group to that of the PBS group at the same time point.

4.8. Cellular Uptake and Co-Localization by Fluorescence Microscopy

Logarithmically growing HGC-27 cells were seeded on coverslips in 12-well plates at 1 × 10^5 cells/well and cultured overnight to allow adherence. DiI-labeled KDNVs were loaded with FAM-labeled si-GPAA1 by electroporation as described in Section 4.6, and the complexes were diluted in PBS to a final siRNA concentration of 100 nM and a KDNV protein concentration of 30 μg/mL. The complexes were added to the cells and incubated for 24 h. After three washes with cold PBS to remove unbound vesicles, cells were fixed with 4% paraformaldehyde for 15 min at room temperature and permeabilized. Nuclei were counterstained with DAPI (1 μg/mL) for 5 min. Coverslips were mounted with anti-fade mounting medium, and the intracellular distribution and co-localization of KDNVs (red fluorescence, DiI) and si-GPAA1 (green fluorescence, FAM) were examined by fluorescence microscopy.

4.9. Western Blotting for GPAA1 Knockdown Efficiency

HGC-27 cells were treated with KDNVs-si-NC, KDNVs-si-GPAA1 or KDNVs-si-GPAA1-RGD for 48 h. Total protein was extracted in RIPA lysis buffer containing protease inhibitors and quantified by the BCA method. Equal amounts of protein (30 μg) were separated by 12% SDS-PAGE and transferred onto PVDF membranes. After blocking with 5% non-fat milk for 1–2 h, the membranes were incubated overnight at 4 °C with primary antibodies against GPAA1 (1:1000) and GAPDH (1:2000), washed with TBST and incubated with the corresponding secondary antibodies for 1 h at room temperature. Protein bands were visualized with a chemiluminescence imaging system, with GAPDH as the loading control.

4.10. RT-qPCR Analysis of GPAA1 mRNA Expression

Total RNA was extracted from HGC-27 cells with TRIzol reagent (Invitrogen, Thermo Fisher Scientific, Carlsbad, CA, USA) following the manufacturer's protocol, and 1 μg of total RNA was reverse-transcribed into cDNA with the PrimeScript RT reagent Kit with gDNA Eraser (Takara, Shiga, Japan). RT-qPCR was run on a

QuantStudio 3 Real-Time PCR System (Applied Biosystems, Waltham, MA, USA) with TB Green Premix Ex Taq II (Tli RNase H Plus) (Takara, Shiga, Japan), under initial denaturation at 95 °C for 30 s, followed by 40 cycles of 95 °C for 5 s and 60 °C for 30 s. The primers were as follows: *GPAA1* forward, 5′-CCT GAA GGT GCT GGT GCT CA-3′; *GPAA1* reverse, 5′-GGA GGC GAT GAC AAA GGT GA-3′; GAPDH forward, 5′-GGA GCG AGA TCC CTC CAA AAT-3′; GAPDH reverse, 5′-GGC TGT TGT CAT ACT TCT CAT GG-3′. Relative *GPAA1* mRNA expression was calculated by the $2^{-\Delta\Delta Ct}$ method and normalized to GAPDH. All assays were performed with three independent biological replicates (n = 3), each analyzed in technical triplicates.

4.11. Transwell Migration and Invasion Assays

For the migration assay, HGC-27 cells treated as indicated were resuspended in serum-free medium and seeded into the upper chambers of Transwell inserts (8 μm pore size) at 3×10^5 cells/well, while a medium containing 10% FBS was placed in the lower chambers as a chemoattractant. After incubation for 24 h, the inserts were removed, fixed with methanol, and stained with crystal violet, and migrated cells were counted under a microscope in five randomly selected fields. For the invasion assay, the upper chambers were pre-coated with Matrigel and the remaining procedures were identical to the migration assay, except that the incubation time was extended to 48 h.

4.12. Statistical Analysis

Statistical analysis was performed with IBM SPSS Statistics software, version 22.0 (IBM Corp., Armonk, NY, USA). Quantitative data are presented as the mean ± standard deviation (SD). All cellular and biochemical experiments were conducted with at least three independent biological replicates (n = 3), each assay measured in technical triplicates. Differences between two groups were evaluated with an unpaired two-tailed Student's *t*-test, and comparisons among multiple groups by one-way analysis of variance (ANOVA) followed by the Student–Newman–Keuls (SNK) test for pairwise post hoc comparisons. A value of $p < 0.05$ was considered statistically significant.

4.13. Use of Generative Artificial Intelligence

The authors used ChatGPT (GPT-6, OpenAI) solely for language editing and proofreading during the preparation of this manuscript. The authors reviewed the suggested edits and take full responsibility for the final published content. No generative AI tools were used to generate or modify research data, figures, or images.

5. Conclusions

In this study, *GPAA1* was confirmed to be overexpressed in GC, where its expression tracked that of the GPI transamidase complex and of extracellular vesicle markers, and kiwifruit-derived exosome-like nanoparticles (KDNVs) were isolated and characterized. In the normal gastric epithelial cell line GES-1, the unloaded vesicles and the RGD-modified vesicles produced no obvious cytotoxic effect, as judged by Annexin V-FITC/PI staining and by CCK-8 measurement of metabolic activity. The particles were internalized efficiently by HGC-27 cells, and silenced *GPAA1* at both the mRNA and protein levels, thereby inhibiting the migration and invasion of GC cells in vitro. RGD modification further improved delivery efficiency and the inhibitory effect. Engineered KDNVs therefore represent a promising natural nanocarrier for targeted gene therapy of GC.

Author Contributions: Conceptualization, X.Z. (Xiaoxin Zhang) and X.Z. (Xu Zhang); methodology, T.S. and L.Z.; software, Q.H. and M.W.; validation, Y.H. and W.J.; formal analysis, T.S., L.Z.

and Q.H.; investigation, Y.H., W.J., C.L., M.W., C.N. and G.G.; resources, X.Z. (Xu Zhang); data curation, J.Z. and R.J.; writing—original draft preparation, X.Z. (Xiaoxin Zhang); writing—review and editing, X.Z. (Xiaoxin Zhang), T.S., L.Z., Y.H., W.J., Q.H., C.L., M.W., C.N., G.G., J.Z., R.J., M.F. and X.Z. (Xu Zhang); visualization, T.S. and Q.H.; supervision, X.Z. (Xu Zhang); project administration, X.Z. (Xiaoxin Zhang) and X.Z. (Xu Zhang); funding acquisition, X.Z. (Xiaoxin Zhang) and X.Z. (Xu Zhang). All authors have read and agreed to the published version of the manuscript.

Funding: This research was funded by the National Natural Science Foundation of China (No. 82103648); the China Postdoctoral Science Foundation (Nos. 2022M711386 and 2025M772008); the Hong Kong Scholars Program (No. XJ2022046); the Natural Science Research Program of Jiangsu Universities (No. 21KJB320013); the Natural Science Foundation of Jiangsu Province (No. BK20240502); the Zhenjiang Science and Technology Planning Project (No. JC2025023); the Basic Research Youth Program of the Zhenjiang Science and Technology Plan (No. JC2025045); the Undergraduate Innovation Training Program of Jiangsu University (No. S202610299098); and the 25th Student Research Project of Jiangsu University (No. 25A211).

Institutional Review Board Statement: Not applicable.

Informed Consent Statement: Not applicable.

Data Availability Statement: The data analyzed in this study are available from The Cancer Genome Atlas (TCGA) and other publicly available databases, as described in the manuscript. Further inquiries can be directed to the corresponding authors.

Conflicts of Interest: The authors declare no conflicts of interest.

Abbreviations

The following abbreviations are used in this manuscript:

BCA	Bicinchoninic Acid
ANOVA	Analysis of Variance
CI	Confidence Interval
CIN	Chromosomal Instability
DMEM	Dulbecco's Modified Eagle Medium
DMSO	Dimethyl Sulfoxide
EGFR	Epidermal Growth Factor Receptor
EV	Extracellular Vesicle
FBS	Fetal Bovine Serum
GC	Gastric Cancer
GPAA1	GPI Anchor Attachment Protein 1
GPI	Glycosylphosphatidylinositol
KDNVs	Kiwifruit-Derived Exosome-Like Nanoparticles
KEVs	Kiwifruit-Derived Extracellular Vesicles
NTA	Nanoparticle Tracking Analysis
PELNs	Plant-Derived Exosome-Like Nanoparticles
PVDF	Polyvinylidene Fluoride
RGD	Arg-Gly-Asp
RNAi	RNA Interference
ROS	Reactive Oxygen Species
RT-qPCR	Reverse Transcription Quantitative PCR
SDS-PAGE	Sodium Dodecyl Sulfate-Polyacrylamide Gel Electrophoresis

siRNA	Small Interfering RNA
SNK	Student–Newman–Keuls
TBST	Tris-Buffered Saline with Tween 20
TCGA	The Cancer Genome Atlas
TEM	Transmission Electron Microscopy
TPM	Transcripts Per Million
TRAIL	TNF-Related Apoptosis-Inducing Ligand

References

1. Sung, H.; Filho, A.M.; Laversanne, M.; Ferlay, J.; Siegel, R.L.; Soerjomataram, I.; Jemal, A.; Bray, F. Global cancer statistics 2024: GLOBOCAN estimates of incidence and mortality worldwide for 34 cancers in 186 countries. *CA Cancer J. Clin.* **2026**, *76*, e70090. [Google Scholar] [CrossRef] [PubMed]
2. Wang, Z.; Han, W.; Xue, F.; Zhao, Y.; Wu, P.; Chen, Y.; Yang, C.; Gu, W.; Jiang, J. Nationwide gastric cancer prevention in China, 2021–2035: A decision analysis on effect, affordability and cost-effectiveness optimisation. *Gut* **2022**, *71*, 2391–2400. [Google Scholar] [CrossRef] [PubMed]
3. Zheng, R.; Zhang, S.; Zeng, H.; Wang, S.; Sun, K.; Chen, R.; Li, L.; Wei, W.; He, J. Cancer incidence and mortality in China, 2016. *J. Natl. Cancer Cent.* **2022**, *2*, 1–9. [Google Scholar] [CrossRef] [PubMed]
4. Smyth, E.C.; Nilsson, M.; Grabsch, H.I.; van Grieken, N.C.; Lordick, F. Gastric cancer. *Lancet* **2020**, *396*, 635–648. [Google Scholar] [CrossRef] [PubMed]
5. Zhang, X.-X.; Ni, B.; Li, Q.; Hu, L.-P.; Jiang, S.-H.; Li, R.-K.; Tian, G.-A.; Zhu, L.-L.; Li, J.; Zhang, X.-L.; et al. GPAA1 promotes gastric cancer progression via upregulation of GPI-anchored protein and enhancement of ERBB signaling pathway. *J. Exp. Clin. Cancer Res.* **2019**, *38*, 214. [Google Scholar] [CrossRef] [PubMed]
6. Wu, G.; Guo, Z.; Chatterjee, A.; Huang, X.; Rubin, E.; Wu, F.; Mambo, E.; Chang, X.; Osada, M.; Kim, M.S.; et al. Overexpression of glycosylphosphatidylinositol (GPI) transamidase subunits phosphatidylinositol glycan class T and/or GPI anchor attachment 1 induces tumorigenesis and contributes to invasion in human breast cancer. *Cancer Res.* **2006**, *66*, 9829–9836. [Google Scholar] [CrossRef] [PubMed]
7. Ho, J.C.; Cheung, S.T.; Patil, M.; Chen, X.; Fan, S.T. Increased expression of glycosyl-phosphatidylinositol anchor attachment protein 1 (GPAA1) is associated with gene amplification in hepatocellular carcinoma. *Int. J. Cancer* **2006**, *119*, 1330–1337. [Google Scholar] [CrossRef] [PubMed]
8. Zhang, J.-X.; Wang, J.-H.; Sun, X.-G.; Hou, T.-Z. GPAA1 promotes progression of childhood acute lymphoblastic leukemia through regulating c-myc. *Eur. Rev. Med. Pharmacol. Sci.* **2020**, *24*, 4931–4939. [Google Scholar] [PubMed]
9. Peer, D.; Karp, J.M.; Hong, S.; Farokhzad, O.C.; Margalit, R.; Langer, R. Nanocarriers as an emerging platform for cancer therapy. *Nat. Nanotechnol.* **2007**, *2*, 751–760. [Google Scholar] [CrossRef] [PubMed]
10. Roviello, G.; Conter, F.U.; Mini, E.; Generali, D.; Traversini, M.; Lavacchi, D.; Nobili, S.; Sobhani, N. Nanoparticle albumin-bound paclitaxel: A big nano for the treatment of gastric cancer. *Cancer Chemother. Pharmacol.* **2019**, *84*, 669–677. [Google Scholar] [CrossRef] [PubMed]
11. Shitara, K.; Takashima, A.; Fujitani, K.; Koeda, K.; Hara, H.; Nakayama, N.; Hironaka, S.; Nishikawa, K.; Makari, Y.; Amagai, K.; et al. Nab-paclitaxel versus solvent-based paclitaxel in patients with previously treated advanced gastric cancer (ABSOLUTE): An open-label, randomised, non-inferiority, phase 3 trial. *Lancet Gastroenterol. Hepatol.* **2017**, *2*, 277–287. [Google Scholar] [CrossRef] [PubMed]
12. Rosenblum, D.; Joshi, N.; Tao, W.; Karp, J.M.; Peer, D. Progress and challenges towards targeted delivery of cancer therapeutics. *Nat. Commun.* **2018**, *9*, 1410. [Google Scholar] [CrossRef] [PubMed]
13. Cai, J.; Qian, K.; Zuo, X.; Yue, W.; Bian, Y.; Yang, J.; Wei, J.; Zhao, W.; Qian, H.; Liu, B. PLGA nanoparticle-based docetaxel/LY294002 drug delivery system enhances antitumor activities against gastric cancer. *J. Biomater. Appl.* **2019**, *33*, 1394–1406. [Google Scholar] [CrossRef] [PubMed]
14. Liu, P.; Yu, H.; Sun, Y.; Zhu, M.; Duan, Y. A mPEG-PLGA-b-PLL copolymer carrier for adriamycin and siRNA delivery. *Biomaterials* **2012**, *33*, 4403–4412. [Google Scholar] [CrossRef] [PubMed]
15. Cong, M.; Tan, S.; Li, S.; Gao, L.; Huang, L.; Zhang, H.-G.; Qiao, H. Technology insight: Plant-derived vesicles—How far from the clinical biotherapeutics and therapeutic drug carriers? *Adv. Drug Deliv. Rev.* **2022**, *182*, 114108. [Google Scholar] [CrossRef] [PubMed]

16. Zheng, Y.; Wang, T.; Zhang, J.; Wei, S.; Wu, Z.; Li, J.; Shi, B.; Sun, Z.; Xu, W.; Zhu, J. Plant-Derived Nanovesicles: A Promising Frontier in Tissue Repair and Antiaging. *J. Agric. Food Chem.* **2025**, *73*, 13159–13177. [Google Scholar] [CrossRef] [PubMed]
17. Gao, Z.; Li, J.; Yang, W.; Gu, Y.; Xu, W.; Liang, Z.; Jiang, J. Plant-Derived Exosome-Like Nanoparticles: Innovative Nanomedicine for Therapeutic Applications. *Food Sci. Nutr.* **2025**, *13*, e70974. [Google Scholar] [CrossRef] [PubMed]
18. Huang, H.; Yi, X.; Wei, Q.; Li, M.; Cai, X.; Lv, Y.; Weng, L.; Mao, Y.; Fan, W.; Zhao, M.; et al. Edible and cation-free kiwi fruit derived vesicles mediated EGFR-targeted siRNA delivery to inhibit multidrug resistant lung cancer. *J. Nanobiotechnology* **2023**, *21*, 41. [Google Scholar] [CrossRef] [PubMed]
19. Liu, H.; Liang, J.; Ye, X.; Huang, M.; Ma, L.; Xie, X.; Liu, D.; Cao, H.; Simal-Gandara, J.; Rengasamy, K.R.R.; et al. The potential role of extracellular vesicles in bioactive compound-based therapy: A review of recent developments. *Crit. Rev. Food Sci. Nutr.* **2023**, *63*, 10959–10973. [Google Scholar] [CrossRef] [PubMed]
20. Yi, C.; Lu, L.; Li, Z.; Guo, Q.; Ou, L.; Wang, R.; Tian, X. Plant-derived exosome-like nanoparticles for microRNA delivery in cancer treatment. *Drug Deliv. Transl. Res.* **2025**, *15*, 84–101. [Google Scholar] [CrossRef] [PubMed]
21. Raimondo, S.; Naselli, F.; Fontana, S.; Monteleone, F.; Dico, A.L.; Saieva, L.; Zito, G.; Flugy, A.; Manno, M.; Di Bella, M.A.; et al. *Citrus limon*-derived nanovesicles inhibit cancer cell proliferation and suppress CML xenograft growth by inducing TRAIL-mediated cell death. *Oncotarget* **2015**, *6*, 19514–19527. [Google Scholar] [CrossRef] [PubMed]
22. Yang, M.; Liu, X.; Luo, Q.; Xu, L.; Chen, F. An efficient method to isolate lemon derived extracellular vesicles for gastric cancer therapy. *J. Nanobiotechnology* **2020**, *18*, 100. [Google Scholar] [CrossRef] [PubMed]
23. Ju, S.; Mu, J.; Dokland, T.; Zhuang, X.; Wang, Q.; Jiang, H.; Xiang, X.; Deng, Z.-B.; Wang, B.; Zhang, L.; et al. Grape exosomelike nanoparticles induce intestinal stem cells and protect mice from DSS-induced colitis. *Mol. Ther.* **2013**, *21*, 1345–1357. [Google Scholar] [CrossRef] [PubMed]
24. Zhang, M.; Viennois, E.; Prasad, M.; Zhang, Y.; Wang, L.; Zhang, Z.; Han, M.K.; Xiao, B.; Xu, C.; Srinivasan, S.; et al. Edible ginger-derived nanoparticles: A novel therapeutic approach for the prevention and treatment of inflammatory bowel disease and colitis-associated cancer. *Biomaterials* **2016**, *101*, 321–340. [Google Scholar] [CrossRef] [PubMed]
25. Zhao, W.-J.; Bian, Y.-P.; Wang, Q.-H.; Yin, F.; Yin, L.; Zhang, Y.-L.; Liu, J.-H. Blueberry-derived exosomes-like nanoparticles ameliorate nonalcoholic fatty liver disease by attenuating mitochondrial oxidative stress. *Acta Pharmacol. Sin.* **2022**, *43*, 645–658. [Google Scholar] [CrossRef] [PubMed]
26. Zhao, Z.; Yu, S.; Li, M.; Gui, X.; Li, P. Isolation of exosome-like nanoparticles and analysis of microRNAs derived from coconut water based on small RNA high-throughput sequencing. *J. Agric. Food Chem.* **2018**, *66*, 2749–2757. [Google Scholar] [CrossRef] [PubMed]
27. Wang, Q.; Zhuang, X.; Mu, J.; Deng, Z.-B.; Jiang, H.; Zhang, L.; Xiang, X.; Wang, B.; Yan, J.; Miller, D.; et al. Delivery of therapeutic agents by nanoparticles made of grapefruit-derived lipids. *Nat. Commun.* **2013**, *4*, 1867, Correction in *Nat. Commun.* **2016**, *7*, 11347.. [Google Scholar] [CrossRef] [PubMed]
28. He, X.; Fang, J.; Chen, X.; Zhao, Z.; Li, Y.; Meng, Y.; Huang, L. Actinidia chinensis Planch.: A Review of Chemistry and Pharmacology. *Front. Pharmacol.* **2019**, *10*, 1236. [Google Scholar] [CrossRef] [PubMed]
29. Fang, Z.; Song, M.; Lai, K.; Cui, M.; Yin, M.; Liu, K. Kiwi-derived extracellular vesicles for oral delivery of sorafenib. *Eur. J. Pharm. Sci.* **2023**, *191*, 106604. [Google Scholar] [CrossRef] [PubMed]
30. Nieberler, M.; Reuning, U.; Reichart, F.; Notni, J.; Wester, H.-J.; Schwaiger, M.; Weinmüller, M.; Räder, A.; Steiger, K.; Kessler, H. Exploring the role of RGD-recognizing integrins in cancer. *Cancers* **2017**, *9*, 116. [Google Scholar] [CrossRef] [PubMed]
31. Gečys, D.; Kazlauskas, A.; Gečytė, E.; Paužienė, N.; Kulakauskienė, D.; Lukminaitė, I.; Jekabsone, A. Internalisation of RGD-engineered extracellular vesicles by glioblastoma cells. *Biology* **2022**, *11*, 1483. [Google Scholar] [CrossRef] [PubMed]
32. Tian, Y.; Li, S.; Song, J.; Ji, T.; Zhu, M.; Anderson, G.J.; Wei, J.; Nie, G. A doxorubicin delivery platform using engineered natural membrane vesicle exosomes for targeted tumor therapy. *Biomaterials* **2014**, *35*, 2383–2390. [Google Scholar] [CrossRef] [PubMed]
33. Johnsen, K.B.; Gudbergsson, J.M.; Skov, M.N.; Pilgaard, L.; Moos, T.; Duroux, M. A comprehensive overview of exosomes as drug delivery vehicles—Endogenous nanocarriers for targeted cancer therapy. *Biochim. Biophys. Acta Rev. Cancer* **2014**, *1846*, 75–87. [Google Scholar] [CrossRef]
34. EL Andaloussi, S.; Lakhal, S.; Mäger, I.; Wood, M.J. Exosomes for targeted siRNA delivery across biological barriers. *Adv. Drug Deliv. Rev.* **2013**, *65*, 391–397. [Google Scholar] [CrossRef] [PubMed]

35. Lu, J.; Chen, J.; Ye, J.; Shi, Z.; Gao, X.; Chen, P.; Chang, Y.; Lin, H.; Li, P. *Dipsacus asperoides*-derived exosomes-like nanoparticles inhibit the progression of osteosarcoma via activating P38/JNK signaling pathway. *Int. J. Nanomed.* **2024**, *19*, 1097–1108. [Google Scholar] [CrossRef] [PubMed]
36. Teng, H.; Zheng, Y.; Cao, H.; Huang, Q.; Xiao, J.; Chen, L. Enhancement of bioavailability and bioactivity of diet-derived flavonoids by application of nanotechnology: A review. *Crit. Rev. Food Sci. Nutr.* **2023**, *63*, 378–393. [Google Scholar] [CrossRef] [PubMed]
37. Lu, X.; Wang, C.; Zhao, M.; Wu, J.; Niu, Z.; Zhang, X.; Simal-Gandara, J.; Süntar, I.; Jafari, S.M.; Qiao, X.; et al. Improving the bioavailability and bioactivity of garlic bioactive compounds *via* nanotechnology. *Crit. Rev. Food Sci. Nutr.* **2022**, *62*, 8467–8496. [Google Scholar] [CrossRef] [PubMed]
38. Elmeligy, S.; Hathout, R.M.; Khalifa, S.A.M.; El-Seedi, H.R.; Farag, M.A. Pharmaceutical manipulation of citrus flavonoids towards improvement of its bioavailability and stability. A mini review and a meta-analysis study. *Food Biosci.* **2021**, *44*, 101428. [Google Scholar] [CrossRef]
39. Feng, Y.; Zhu, Y.; Wan, J.; Yang, X.; Firempong, C.K.; Yu, J.; Xu, X. Enhanced oral bioavailability, reduced irritation and increased hypolipidemic activity of self-assembled capsaicin prodrug nanoparticles. *J. Funct. Foods* **2018**, *44*, 137–145. [Google Scholar] [CrossRef]
40. Wang, Q.; Wang, Y.; Xie, Y.; Adu-Frimpong, M.; Wei, C.; Yang, X.; Cao, X.; Deng, W.; Toreniyazov, E.; Ji, H.; et al. Nonionic surfactant vesicles as a novel drug delivery system for increasing the oral bioavailability of Ginsenoside Rb1. *Food Biosci.* **2021**, *42*, 101064. [Google Scholar] [CrossRef]
41. Chen, Q.; Fang, Z.; Yang, Z.; Xv, X.; Yang, M.; Hou, H.; Li, Z.; Chen, Y.; Gong, A. *Lactobacillus plantarum*-Derived Extracellular Vesicles Modulate Macrophage Polarization and Gut Homeostasis for Alleviating Ulcerative Colitis. *J. Agric. Food Chem.* **2024**, *72*, 14713–14726. [Google Scholar] [CrossRef] [PubMed]
42. Zhuang, X.; Teng, Y.; Samykutty, A.; Mu, J.; Deng, Z.; Zhang, L.; Cao, P.; Rong, Y.; Yan, J.; Miller, D.; et al. Grapefruit-derived nanovectors delivering therapeutic miR17 through an intranasal route inhibit brain tumor progression. *Mol. Ther.* **2016**, *24*, 96–105. [Google Scholar] [CrossRef] [PubMed]
43. Zhang, M.; Wang, X.; Han, M.K.; Collins, J.F.; Merlin, D. Oral administration of ginger-derived nanolipids loaded with siRNA as a novel approach for efficient siRNA drug delivery to treat ulcerative colitis. *Nanomedicine* **2017**, *12*, 1927–1943. [Google Scholar] [CrossRef] [PubMed]
44. Choi, H.S.; Liu, W.; Misra, P.; Tanaka, E.; Zimmer, J.P.; Ipe, B.I.; Bawendi, M.G.; Frangioni, J.V. Renal clearance of quantum dots. *Nat. Biotechnol.* **2007**, *25*, 1165–1170. [Google Scholar] [CrossRef] [PubMed]
45. Ernsting, M.J.; Murakami, M.; Roy, A.; Li, S.-D. Factors controlling the pharmacokinetics, biodistribution and intratumoral penetration of nanoparticles. *J. Control. Release* **2013**, *172*, 782–794. [Google Scholar] [CrossRef] [PubMed]
46. Zeng, H.; Guo, S.; Ren, X.; Wu, Z.; Liu, S.; Yao, X. Current strategies for exosome cargo loading and targeting delivery. *Cells* **2023**, *12*, 1416. [Google Scholar] [CrossRef] [PubMed]
47. Danilushkina, A.A.; Emene, C.C.; Barlev, N.A.; Gomzikova, M.O. Strategies for engineering of extracellular vesicles. *Int. J. Mol. Sci.* **2023**, *24*, 13247. [Google Scholar] [CrossRef] [PubMed]
48. Valadi, H.; Ekström, K.; Bossios, A.; Sjöstrand, M.; Lee, J.J.; Lötvall, J.O. Exosome-mediated transfer of mRNAs and microRNAs is a novel mechanism of genetic exchange between cells. *Nat. Cell Biol.* **2007**, *9*, 654–659. [Google Scholar] [CrossRef] [PubMed]
49. Lamichhane, T.N.; Raiker, R.S.; Jay, S.M. Exogenous DNA loading into extracellular vesicles via electroporation is size-dependent and enables limited gene delivery. *Mol. Pharm.* **2015**, *12*, 3650–3657. [Google Scholar] [CrossRef] [PubMed]

Disclaimer/Publisher's Note: The statements, opinions and data contained in all publications are solely those of the individual author(s) and contributor(s) and not of MDPI and/or the editor(s). MDPI and/or the editor(s) disclaim responsibility for any injury to people or property resulting from any ideas, methods, instructions or products referred to in the content.